Chapter 7
Heat and Electro-Responsive Nanomaterials for Smart Windows

Jiadong Qin and Yu Lin Zhong

Abstract Energy-saving buildings have drawn increasing interest worldwide in the past 30 years, during which the growing population and expanding urbanization significantly increased the energy intensity of numerous cities. In the modern energy-saving buildings, smart windows are playing an important role in the efficient utilization of daylight and the intelligent control of heat exchange between indoor and outdoor, eventually reducing the energy waste associated with lighting and air-conditioning. The "intelligence" of smart windows originates from the responsive materials of which the optical properties are adaptive to temperature or applied voltage. Recently, the development of smart windows has been greatly motivated by the burgeoning nanomaterials. This chapter focuses on the development of heat and electro-responsive nanomaterials-based smart windows which outperform the conventional ones and, more importantly, likely to cost less for commercialization.

7.1 Introduction

The residential, public and commercial buildings consume considerable energy for heating, ventilation and air conditioning (HVAC) but more than 50% of the energy use is wasted due to the unwanted heat exchange through the conventional windows [1]. Additionally, due to the poor utilization of daylight, the maintenance of interior brightness still relies on the lightings even in the daytime. To reduce the unnecessary energy waste, smart windows are regarded as an efficient and promising energy conservation technology as they can dynamically adapt the heat flux and the light transmission to the changing exterior temperature and sunlight intensity. Furthermore, smart windows, through flexible switchability between a transparent state and an opaque state, can provide privacy protection and the control over indoor brightness

J. Qin · Y. L. Zhong (✉)
Centre for Clean Environment and Energy, School of Environment and Science, Griffith University, Gold Coast Campus, Gold Coast, QLD 4222, Australia
e-mail: y.zhong@griffith.edu.au

Z. Sun and T. Liao (eds.), *Responsive Nanomaterials for Sustainable Applications*, Springer Series in Materials Science 297,
https://doi.org/10.1007/978-3-030-39994-8_7

and temperature. Therefore, smart windows will eliminate the needs for curtains or blinds and provide additional controls.

The core of smart windows lies in the chromogenic materials whose transmittance is in response to the external stimuli, such as temperature (thermochromic) and applied voltage (electrochromic). Currently, thermochromic and electrochromic materials are playing the dominant roles in the smart windows. The temperature-responsive thermochromic windows are one of the most-studied smart windows as they can reduce the influx of heat in hot weather but welcome the heat from sunlight in cold weather. The principle is that the thermochromic materials can undergo a reversible phase transition or chemical reaction at a well-defined critical temperature (T_c). This will significantly change their optical properties to the near-infrared (NIR) light in the spectral range of 780–2500 nm, which is the predominant contributor of solar heat. They can block the NIR light at high temperature above T_c, whereas allowing the traverse of IR light at low temperature below T_c (as illustrated in Fig. 7.1a). Therefore, thermochromic windows with well-controlled heat exchange ability are helpful to reduce the energy consumption by HVAC. Electrochromic windows are another attractive type of smart windows. They can reversibly switch between coloured and bleached state, responsive to the applied voltage. A typical electrochromic window is based on an electrochemical cell structure where the active electrochromic components and the electrolyte layer are sandwiched between two transparent conducting electrodes (TCEs), as shown in Fig. 7.1b. When the device is switched on, the external voltage propels the migration of electric charges from the counter electrode, through the electrolyte, to the electrochromic electrode, giving rise to the change in its oxidation state and hence, the corresponding colouration [2]. When switched off, electric charges move back to the counter electrode for charge balance, and the electrochromic electrode concurrently reverts to its original bleached state. Electrochromic windows behave like an electrical curtain which facilitates the flexible broadband modulation of light transmittance [3].

Commercial smart windows have already emerged in the market. One of the best-known examples is the electrochromic windows employed in the Boeing 787 Dreamliner aeroplane, which can gradually darken under the external bias. Though advantageous in the improved energy conservation and dynamic energy management, smart windows fail to make a greater impact in the building market at the present stage because the conventional chromogenic materials are limited by high cost, inconsistent chromogenic ability as well as questionable working life. Fortunately, the recent promising researches in nanomaterials are likely to revive the commercialized smart windows in the near future. The functionality, reliability and stability of smart windows can be further improved by nanomaterials and nanostructuring via the facile and precise controls of morphology, nanocrystal size, surface chemistry and composition. Also, the employment of nanomaterials will benefit the scalable and cost-efficient manufacturing of smart windows. This is because a wide range of nanomaterials and their synthesis routes are solution-processable and free from high-temperature treatment [3]. Apart from the conventional methods (roll-to-roll printing and bar coating), many chromogenic nanomaterials can be deposited onto glass to form the “intelligently” responsive layers using the three-dimensional

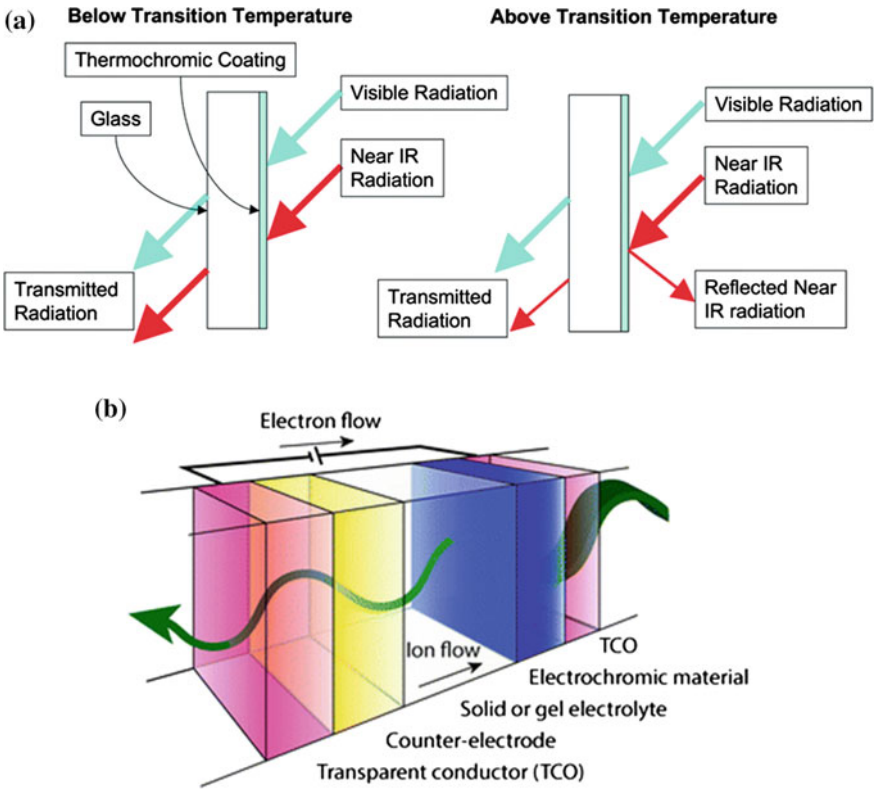

Fig. 7.1 Schematic mechanism of thermochromic and electrochromic windows. **a** For the thermochromic windows, the active thermochromic coating has a critical transition temperature. Below the transition temperature, most of the NIR light can pass through the window, thus transferring the solar heat into the building (keep the interior warm). However, the NIR light will be blocked outdoors above the transition temperature, which greatly reduces the transmitted heat radiation (keep the interior cool). Reproduction from [4] with permission from Royal Society of Chemistry, Copyright 2014. **b** When applying the voltage, the flowing ions will cause the reversible chromogenic reaction in the electrochromic layers, contributing the colour changes. Reproduction from [2] with permission from Royal Society of Chemistry, Copyright 2014

(3D) printing techniques [5–7]. With the advantages in the reproducible and customizable fabrication, the low-cost 3D printed smart windows show great promise in standardization and commercialization.

In this chapter, we review the recent progress in the responsive nanomaterials for smart windows. In Sects. 7.2 and 7.3, we focus on the nanomaterials-based thermochromic and electrochromic windows, respectively, from the perspective of working principles, light management ability and device engineering. Finally, to provide an outlook for the commercialization of smart windows, we discuss the importance of the utilization of nanomaterials and the challenges to be solved for the crucial laboratory-to-industries transition in Sect. 7.4.

7.2 Responsive Nanomaterials for Thermochromic Smart Windows

Temperature-responsive thermochromic smart windows can switch between the NIR-transparent and -blocking state at the transition temperature of T_c to realize the dynamic regulation of heat flux through the windows. For an ideal thermochromic smart window, it should simultaneously have high solar energy modulation ability ΔT_{solar} and high visible light transmittance (also known as luminous transmittance T_{lum} in the spectral range of 380–780 nm). In terms of ΔT_{solar}, it is the difference in the transmittance of solar energy, T_{solar}, between the two states in the range of 240–2500 nm, indicative of the energy conservation efficiency [8]. Apart from that, a suitable T_c in close proximity to room temperature (25–30 °C) is also needed for more effective thermal management. Besides the optical performance, thermochromic smart windows must be mechanically robust and chemically inert due to their long-time exposure to the weather.

Major conventional thermochromic windows make use of thermochromic polymers or inorganic solids to modulate the light transmission and the associated heat exchange [9, 10]. The advancement in nanomaterial science not only revitalizes the conventional materials but also introduces some new materials and novel device design with improved performance. Here, we discuss some of the representative thermochromic nanomaterials for smart windows.

7.2.1 Vanadium Dioxide-Based Thermochromic Nanomaterials

Among all of the conventional thermochromic materials, vanadium dioxide (VO_2) has attracted the most extensive studies due to its unique reversible metal-to-insulator transition (MIT) at a relatively low T_c of 68 °C (as shown in Fig. 7.2) and the accompanied abrupt change in the light transmittance in NIR region since the 1980s [12]. Upon exceeding T_c, the occurrence of MIT will immediately transform the crystalline structure of VO_2, from an insulating and NIR-transparent monoclinic phase (M phase, <68 °C) to a metallic and NIR-translucent rutile phase (R phase, >68 °C), within only 10^{-12} s [13]. In contrast, the phase transition of VO_2 does not apparently affect the transmittance of visible light (no obvious colour change) [8]. The T_c of VO_2 can be effectively reduced by elemental doping, such as H [14], W [15] and Mo [16], which makes VO_2 more applicable for practical use. This thermochromism behaviour, therefore, enables the temperature-adaptive regulation of solar heat. Nevertheless, the VO_2-based smart windows are limited by the poor ΔT_{solar} and T_{lum}, less than 20% and 50%, respectively [17]. The bigger challenge is that ΔT_{solar} and T_{lum} are seemingly mutually exclusive because it is difficult to enhance both parameters simultaneously [8]. In the traditional approach, T_{lum} can be improved by reducing the thickness of VO_2-based continuous film but at the expense

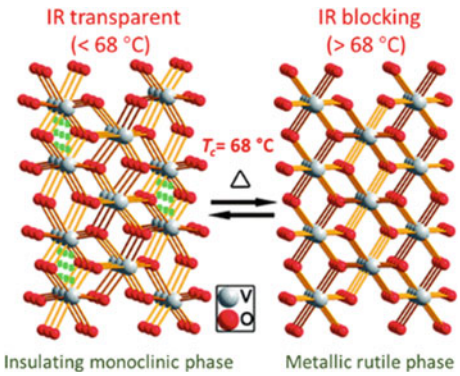

Fig. 7.2 Schematic of the change in the crystal structure of VO_2 at the T_c of 68 °C. When heated to 68 °C, the insulating monoclinic VO_2 (IR transparent) will transform into the metallic rutile phase with longer V-V distance (IR blocking). Conversely, the rutile VO_2 can recover to the monoclinic phase as cooled to below T_c. Reproduction from [11] with permission from Royal Society of Chemistry, Copyright 2011

of ΔT_{solar}, as illustrated in Fig. 7.3 [18]. Another approach to enhancing T_{lum} of VO_2 film is to apply the antireflection coatings and form the multilayered structures which utilize the light interference between the film interfaces [19]. However, the introduction of antireflection coatings normally requires the expensive and complex physical vapour deposition technology [20–22]. To fulfil the great potential of VO_2 for smart windows, a number of researches have attempted to achieve the optimal thermochromic properties, especially ΔT_{solar} and T_{lum} [8], via the forming of VO_2-based nanocomposites [23, 24] and the nanostructuring of VO_2 [25, 26].

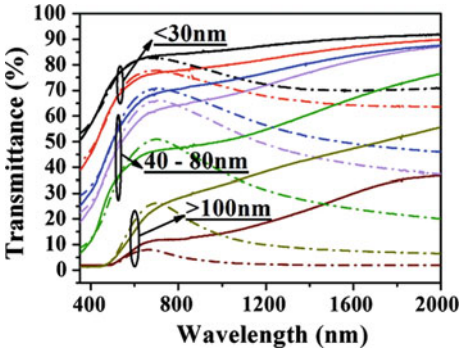

Fig. 7.3 UV-Vis-NIR transmittance spectra for VO_2 continuous films with different thickness. The solid and dashed lines represent the spectra measured at 20 and 90 °C, respectively. It is apparent that an ultrathin VO_2 film (<30 nm) can provide high T_{lum} (~80%) but low ΔT_{solar} (~20%). With the increased film thickness (>100 nm), ΔT_{solar} was noticeably enhanced (~50%) while T_{lum} was dropped sharply (~10%). Reproduction from [27] with permission from American Chemical Society, Copyright 2010

Relative to the bulk particles, the nanosized VO_2 particles (<40 nm) with high crystallinity and uniform sizes have better dispersibility in the aqueous solvent, in favour of the low-cost solution processing [28, 29]. The facile dispersion will greatly facilitate the forming of nanocomposites by dispersing the VO_2 nanocrystals into the dielectric matrix, such as polyurethane (PU) [30] and polydimethylsiloxane (PDMS) [31]. The VO_2-based nanocomposites, attributed to the minimized Mie scattering [32], can offer higher solar modulation ability as well as visible transmittance than the continuous VO_2 thin films, which was first demonstrated by the theoretical calculation [33]. As compared to the simulated spectral transmittance in Fig. 7.4a, b, the dispersive VO_2 nanocomposite can simultaneously achieve larger ΔT_{solar} and T_{lum} than the continuous film. On top of that, the particle size-dependent optical properties, which are obvious in Fig. 7.4a, imply the smaller VO_2 particles are more favourable for high ΔT_{solar} and T_{lum} [33]. Further, the advantages of the nanocomposite film have been confirmed by the practical experiments [8, 30, 31]. For example, Chen et al. reported a VO_2-based nanocomposite foil comprised of uniformly dispersed VO_2 nanoparticles in the PU matrix, as shown in Fig. 7.4c–e [30]. This type of nanocomposite film can deliver excellent optical properties ($\Delta T_{solar} = 22.3\%$ and $T_{lum} = 45.6\%$), which was superior to the continuous thin film [27], and VO_2-based multilayered film [34]. Because VO_2 is prone to be oxidized into V_2O_5 in the ambient air, VO_2 nanoparticles are usually coated with a stable oxide layer, such as SiO_2 [28] and ZnO [35], to form an oxidation-resistant core-shell structure. The model of dispersive VO_2-based nanocomposites also works well on the thin-walled VO_2 nanoparticles, providing an even higher ΔT_{solar} only at the cost of a slightly lesser T_{lum} [36]. Another advantage of scaling to nanometre-sized dimensions is that the thermochromic performance can also benefit from the localized surface plasmon resonance (LSPR) of the metallic VO_2 (R) nanoparticles [37]. The LSPR, initiated by the coupling of the resonance frequency of free electrons in VO_2 (R) with the wavelength of the incident light [38], will give rise to strong absorption in the NIR range and hence the enhanced ΔT_{solar} [39–42]. In addition to the improved optical properties, VO_2 nanoparticles are more resilient to the MIT-induced strain in the lattice, which guarantees the mechanical stability of thin films [43].

The optical properties of the VO_2 film can also be improved by the introduction of nanopores, of which the sizes are far smaller than the visible wavelength [25, 44–46]. Similar to the dispersive VO_2 nanocomposite, trapped air in the nanopores acts as a secondary phase. According to the simulated thermochromic performance (Fig. 7.5a), Zhang and his co-workers demonstrated that the increased porosity can enhance ΔT_{solar} of the nanoporous VO_2 films without the sacrifice of T_{lum} due to the higher ability to depress the reflection [25]. They also fabricated the VO_2 film with random porosity (pore size: 15–80 nm) by incorporating the removable polymer additives, and the resulting nanoporous film ($T_{lum} = 43.3\%$, $\Delta T_{solar} = 14.1\%$, Fig. 7.5b) had comparable optical performance to the multilayered VO_2 film with the optically optimized structure ($T_{lum} = 44\%$, $\Delta T_{solar} = 12\%$) [25]. In contrast to the random porous films, the highly ordered porosity can further improve the performance. For instance, Zhou et al. first reported the fabrication of periodic nanoporous VO_2 film, which featured a grid-like structure (Fig. 7.5c), using a feasible colloid lithography

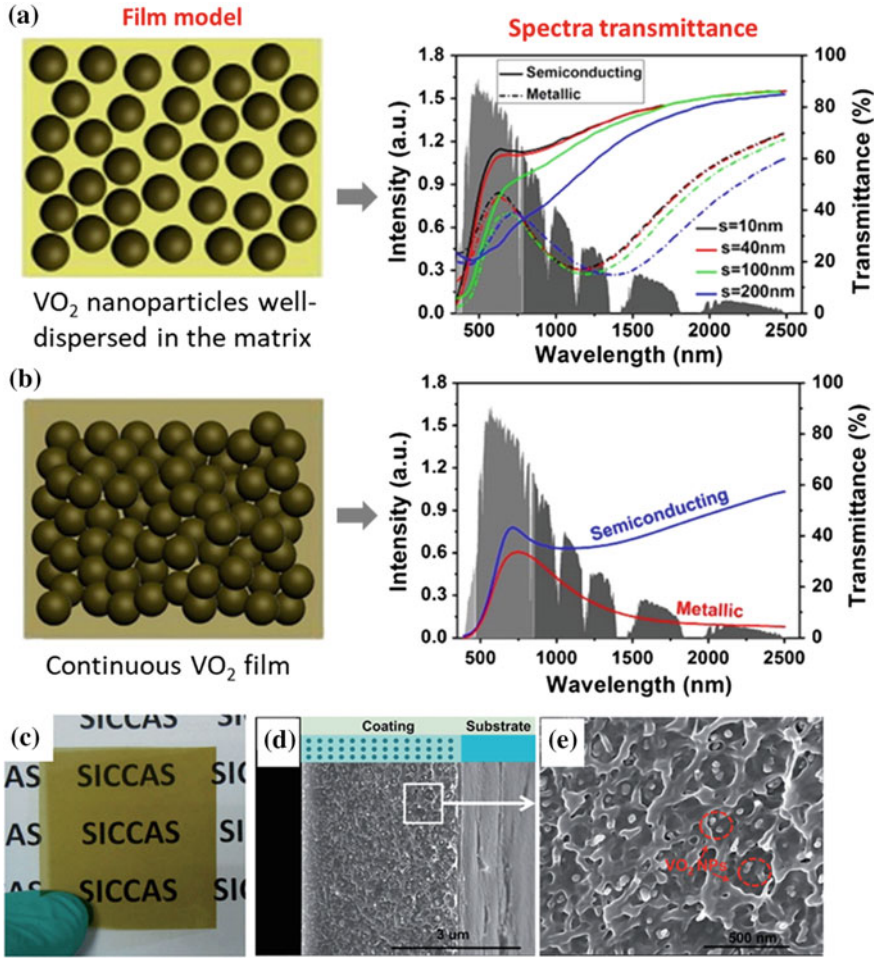

Fig. 7.4 Simulated and the experimental dispersive VO_2 nanocomposites. The ideal film models and their simulated light transmittance spectra for **a** a nanocomposite in which VO_2 nanoparticles (with different sizes: 10, 40, 100 and 200 nm, filling factor = 0.01) are uniformly embedded and **b** the continuous film in which the VO_2 nanoparticles cluster together. With the same film thickness of 10 μm, the dispersive VO_2 nanocomposite obviously has advantages in high ΔT_{solar} and T_{lum} over the continuous film. **a**, **b** Reproduction from [40] with permission from American Chemical Society, Copyright 2015. **c** The image of the nanocomposite-coated glass which shows a yellowish green colour. The composite coating is composed of the dispersed VO_2 nanoparticles in the PU matrix. **d** SEM images of the cross-sectional nanocomposite coating on the substrate and **e** the homogeneous dispersion of VO_2 nanoparticles in the PU matrix. **c**–**e** Reproduction from [30] with permission from Royal Society of Chemistry, Copyright 2014

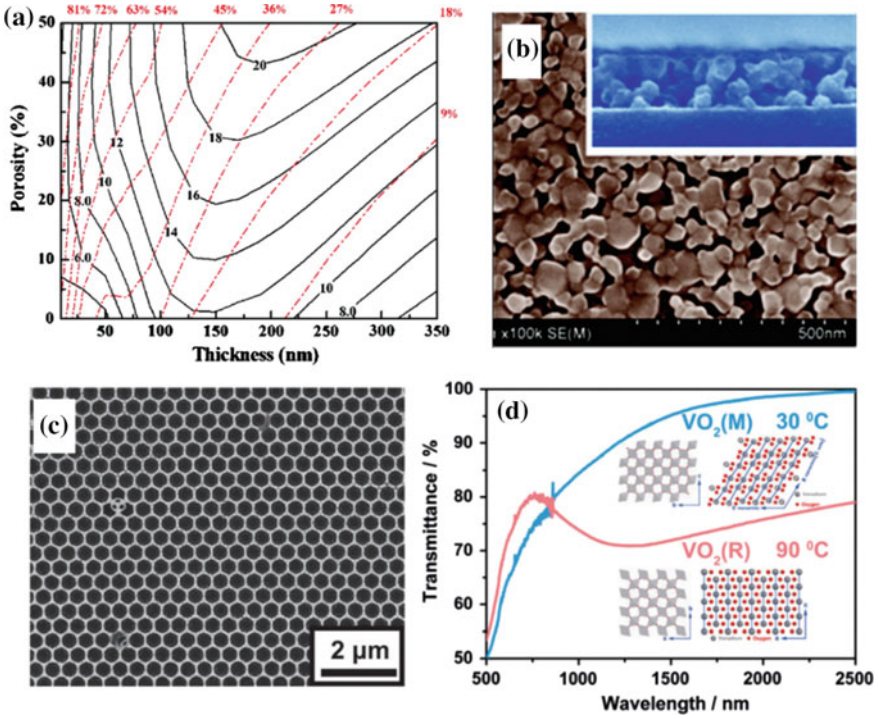

Fig. 7.5 Simulated and experimental optical performance of nanoporous VO_2 film. **a** The calculated T_{lum} of monoclinic VO_2 at low temperature (red dotted lines) and ΔT_{solar} of rutile VO_2 at high temperature(black solid lines) as a function of thickness and porosity of the VO_2 films. **b** SEM image of the VO_2 film with random porosity. The inset is the cross-sectional view of the nanoporous film. **a**, **b** Reproduction from [25] with permission from American Chemical Society, Copyright 2011. **c** SEM image of the single-layered periodic porous VO_2 film. (3) The spectral transmittance of the periodic porous film at low-temperature insulating (M phase, 30 °C) and high-temperature metallic state (R phase, 90 °C). It is apparent that the porous VO_2 highlights the ultrahigh visible transmittance regardless of the phase transition ($T_{lum} > 80\%$). **c**, **d** Reproduction from [45] with permission from Royal Society of Chemistry, Copyright 2014

method [45]. Owing to the optimal space occupancy of monoclinic VO_2 crystals, the periodic porous film possessed ultrahigh visible transmittance ($T_{lum} = 81\%$) and excellent solar modulation ability ($\Delta T_{solar} = 23\%$), as illustrated in Fig. 7.5d [45].

To fabricate the VO_2-based smart windows, the traditional approach is to employ the gas-phase deposition methods, including physical vapour deposition [47–49] and chemical vapour deposition [50–52], to form a uniform and high-quality VO_2 thermochromic film on the glass. However, the expensive and complex gas-phase deposition methods impede the mass production and commercialization of the smart windows. Due to the excellent solution processability, VO_2 nanoparticles are fully compatible with the scalable, low-cost and high-yield solution phase deposition methods, such as sol-gel coating [53, 54] and polymer-assisted deposition [25, 55].

Moreover, the dispersible VO_2 nanoparticles can be exploited as the active components in the thermochromic inks for 3D printed smart windows. In 2018, Ji et al. demonstrated the first inkjet printed VO_2 smart window with desirable performance (ΔT_{solar}= 15.31%) [7]. They carefully tuned the viscosity (8 mPa s) and surface tension (26.8 mN/m) of the ink based on VO_2 nanoparticles (30–50 nm). Therefore, the inks can be continuously deposited onto the glass and then solidify into the compact VO_2 thermochromic film via a simple thermal treatment at 80 °C after printing. This proof-of-concept 3D printed smart window is likely to open up new possibilities for the customizable fabrications of smart windows.

7.2.2 Polymer-Based Thermochromic Nanomaterials

Generally, thermochromism in the polymeric materials originates from the changes in light reflection or absorption induced by the thermally driven structural rearrangement or reversible reaction [3, 9]. In recent years, thermochromic hydrogels, which consist of the water-swollen networks of polymer chains, have emerged as a new class of temperature-responsive materials for smart window application [17, 56]. The solar heat can activate a hydrophilic-to-hydrophobic transition in thermochromic hydrogels, accompanied by the change in transparency, as long as the lower critical solution temperature (LCST) is surpassed (Fig. 7.6a). Below the LCST, intermolecular hydrogen bonds allow the polymer chains to be hydrated and swollen. When heated above the LCST, the breakage of intermolecular hydrogen bonds will cause dehydration of the polymer networks, leading to structural collapse and polymer aggregation [17, 57]. The aggregated polymer chains tend to invite more light scattering, which significantly reduces the transparency of the hydrogels (Fig. 7.6b) [58, 59]. The thermochromic hydrogels include but are not limited to hydroxypropyl cellulose (HPC) [60], polyampholyte hydrogel (PAH) [61] and poly(*N*-isopropylacrylamide) (PNIPAm) [62–64].

Due to the intrinsic cross-linked structure and temperature responsiveness, thermochromic hydrogels act as an ideal switchable matrix for photothermal nanoparticles to form a dual-responsive nanocomposite for smart windows [63]. Typically, the temperature-responsive materials only respond to the surrounding temperature but not the intensity of sunlight. As a result, they fail to provide dimming control in cold climates despite exposure to the intensive sunlight. In comparison, the dual-responsive nanocomposites can sense not only the environmental temperature but also the intensity of solar irradiation. The additional responsiveness to sunlight arises from the conversion of sunlight to heat by the embedded photothermal nanoparticles, such as graphene oxide (GO) and antimony tin oxide (ATO) [63, 66]. Once the converted heat transfers to the hydrogel matrix, the temperature increase will trigger the optical switching from transparent to translucent in the nanocomposite. For example, Lee et al. fabricated such dual-responsive nanocomposites by incorporating ATO nanoparticles into the PNIPAm hydrogel (Fig. 7.7a, b) [63]. When the solar irradiation is sufficiently intensive, the photothermal effect of ATO nanoparticles

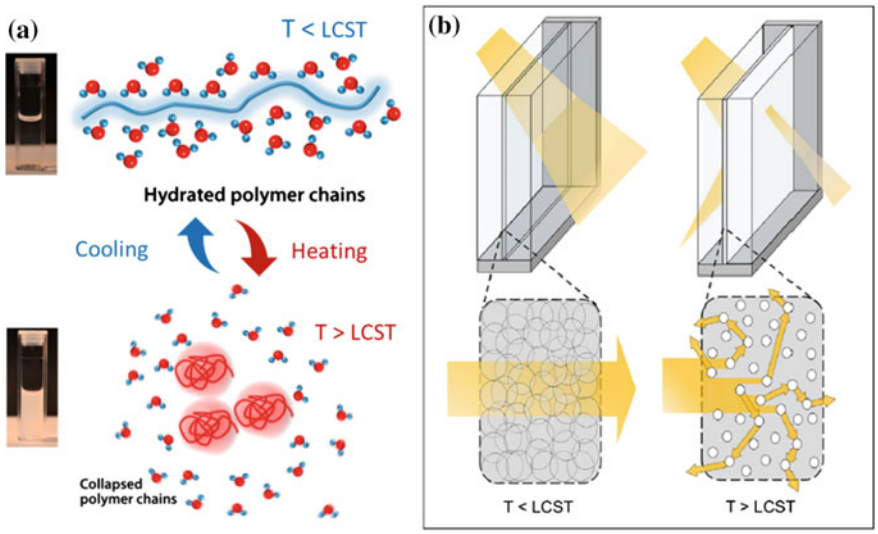

Fig. 7.6 Schematic of thermochromic hydrogels below and above the LCST. **a** The temperature-responsive arrangement of polymer chains. Below the LCST, the hydrophilic polymer chains are surrounded by water molecules and the hydrogel is transparent. Above the LCST, the polymer chains lose water molecules and collapse into polymer clusters which make the hydrogel opaque. Reproduction from [65] with permission from Elsevier, Copyright 2016. **b** The schematic of a smart window where the thermochromic hydrogel layer is sandwiched between two glass panels. The incident light can pass through the hydrogel layer below the LCST but is largely blocked above the LCST due to the light scattering. Reproduction from [42] with permission from Elsevier, Copyright 2019

will enable the immediate phase transition in the PNIPAm, making dimming control feasible even under the LCST of PNIPAm (~32 °C) in less than 5 min, as shown in Fig. 7.7c [63].

In addition to the photothermal nanoparticles, VO_2 nanoparticles can also be hybridized with the thermochromic hydrogel to form the aforementioned dispersive VO_2-based nanocomposite [60, 64]. In 2015, Zhou et al. reported a sandwich-type smart window based on a VO_2/PNIPAm hybrid nanocomposite (Fig. 7.8a, b) [64]. The highlight of their work is that the hybrid nanocomposite can afford excellent thermochromic performance ($T_{lum} = 62.6\%$, $\Delta T_{solar} = 34.7\%$), superior to pure VO_2 nanoparticles and pure PNIPAm hydrogel (Fig. 7.8c). The hybrid system exhibited dramatical contrast in the visible and NIR region, contributing to the prominent enhancement in ΔT_{solar} [64].

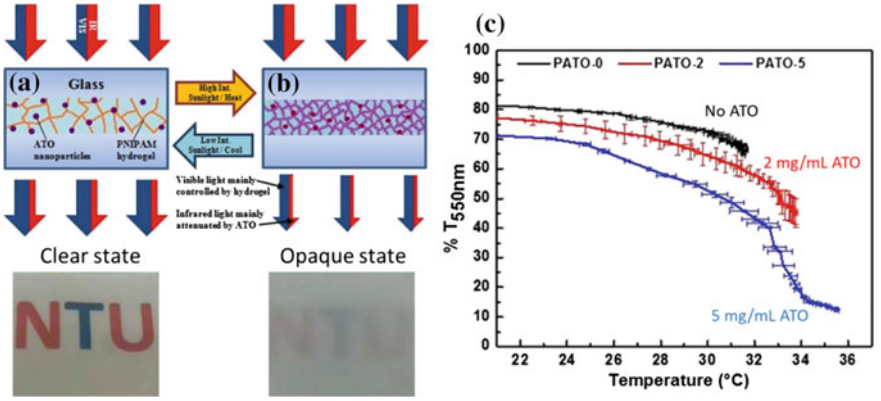

Fig. 7.7 Schematic of the dual-responsive PNIPAm/ATO nanocomposite in **a** clear state and **b** opaque state. The photothermal ATO nanoparticles are evenly distributed in the cross-linked hydrogel networks. Upon exposure to the strong sunlight, the ATO nanoparticles, acting as a nanoheater, convert sunlight to thermal energy, giving rise to temperature increase and phase transition in the PNIPAm. The hydrogel matrix is in charge of the visible light manipulation while the ATO nanoparticles can absorb the NIR light. **c** The optical switching of the nanocomposite is dependent on the content of ATO nanoparticles. With the addition of more ATO nanoparticles, the phase transition of PNIPAm tended to start at a lower temperature under the solar irradiation. Reproduction from [63] with permission from American Chemical Society, Copyright 2017

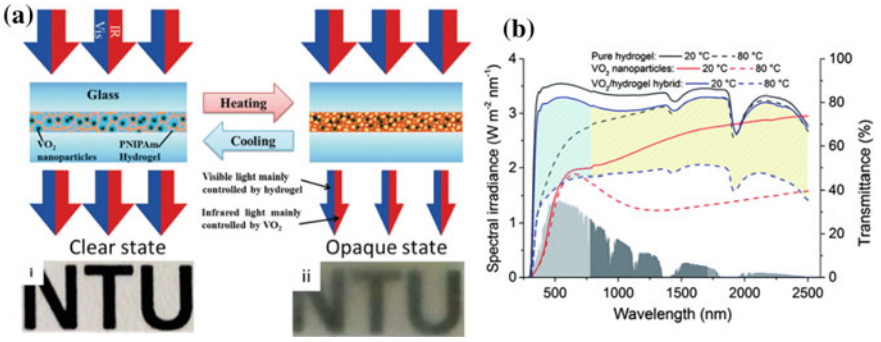

Fig. 7.8 **a** Schematic of the smart window based on the VO_2/PNIPAm nanocomposite. The PNIPAm matrix regulates the visible transmittance at ~30 °C while VO_2 nanoparticles regulate the NIR transmittance at ~68 °C. The insets (i) and (ii) show the clear state at room temperature (hydrated PNIPAm) and opaque state at 35 °C (dehydrated PNIPAm). **b** UV-Vis-NIR transmittance spectra of VO_2/PNIPAm nanocomposite, pure VO_2 nanoparticles and pure PNIPAm at 20 and 80 °C. It is obvious that VO_2/PNIPAm hybrid has higher T_{lum} than pure VO_2 due to the reduced light scattering. Further, VO_2/PNIPAm hybrid has greatly enhanced ΔT_{solar} relative to the other two. Reproduction from [64] with permission from Royal Society of Chemistry, Copyright 2015

7.2.3 *Halide Perovskite-Based Thermochromic Nanomaterials*

Over the past decades, halide perovskites of an ABX_3 crystal structure [A = $CH_3NH_3^+$ (MA), $HC(NH_2)_2^+$ (PA) or Cs^+; B = Pb^{2+}or Sn^{2+}; X = I^-, Br^- and Cl^-] as shown in Fig. 7.9 have been the research hotspots of photovoltaic nanomaterials due to their high-power conversion efficiency and low cost [67–69]. The tremendous research efforts on perovskites not only make huge progress in the photovoltaic devices but open up a new avenue for thermochromic smart windows as well.

In 2017, Bakr's group pioneered the work on the organic halide perovskites-based ($MAPbBr_{3-x}I_x$) thermochromic windows which exhibited yellow, orange, red and black colour at 25, 60, 90 and 120 °C, respectively (Fig. 7.10a, b) [71]. The thermochromism of the perovskite materials is associated with the inverse temperature crystallization (ITC) of halide perovskites, which means their solubility decreases at elevated temperature in certain solvents [72]. Another intriguing aspect is that both the crystallization temperature of ITC and the absorption of photons by the perovskites rely on the halogen constituent of the perovskites [73]. Therefore, with the increment of the temperature, orange $MAPbBr_{2.7}I_{0.3}$, red $MAPbBr_{2.4}I_{0.6}$ and black $MAPbBr_{1.8}I_{1.2}$ perovskite crystals successively precipitate out from the original yellow biconstituent perovskite solution at 60, 90 and 120 °C (Fig. 7.10c). The temperature-dependent precipitation and dissolution of perovskite crystals lead to the reversible chromatic variation.

Most importantly, the use of halide perovskites realizes the perfect combination of sunlight-regulating smart windows and power-generating photovoltaic windows

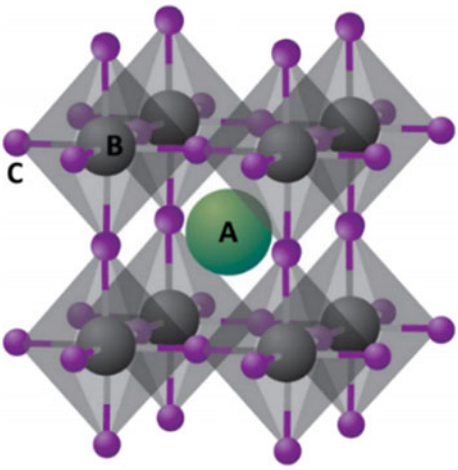

Fig. 7.9 Crystal structure of cubic halide perovskites with the general formula of ABX_3. The larger cation A (green) occupied the cuboctahedral voids formed by the 12 nearest-neighbouring X ions (purple). The smaller cation B is centred at the unit cell. Reproduction from [70] with permission from Nature Publishing Group, Copyright 2014

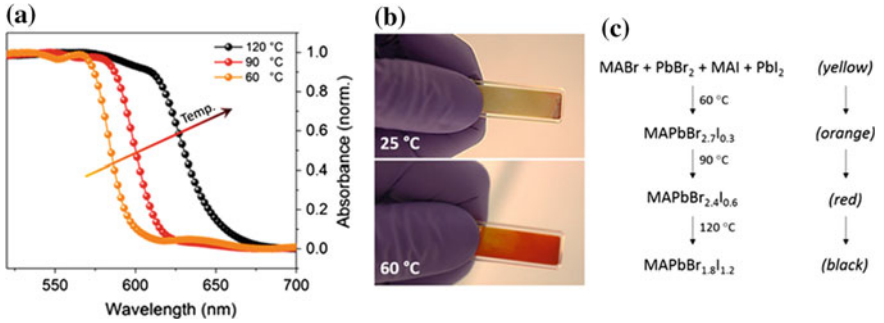

Fig. 7.10 **a** Absorption spectra of thermochromic perovskite crystals obtained at 60, 90 and 120 °C. The original yellow solution changed to orange at 60 °C, to bright red at 90 °C and finally to black at 120 °C. **b** Images of the thermochromic prototype annealed at 25 and 60 °C. **c** The formulation of the original perovskite solution and the major contributors of colour changes at 60, 90 and 120 °C. Reproduction from [71] with permission from American Chemical Society, Copyright 2017

at the same time (smart solar windows). One the one hand, perovskites can efficiently convert sunlight to electricity, as what they do in solar cells. On the other hand, their distinct chemistry and nanostructure render perovskites' optoelectronic properties responsive to the temperature change [74]. Consequently, the smart solar windows literally make full use of solar energy. In 2017, Wheeler et al. fabricated an inorganic–organic hybrid halide perovskite ($MAPbI_3$)-based smart solar window which can rapidly switch between transparent and opaque at 60 °C within a few minutes (Fig. 7.11a) [75]. At cooler temperature, the perovskite forms a visibly transparent complex with the methylamine (CH_3NH_2) in a sealed layer. When the temperature hits 60 °C, the window switches into an opaque state attributed to the dissociation of CH_3NH_2 from the complex and the strong absorption of sunlight by the perovskite (Fig. 7.11b). In the opaque state, the photovoltaic effect of the perovskite enables the transformation of absorbed solar energy into electricity, and the conversion efficiency reaches up to 11.3% (Fig. 7.11c). When cooled below 60 °C, CH_3NH_2 gas returns to the perovskite and reforms the complex, making the window return to the transparent state. Besides the chemical reaction-driven thermochromism, it has been found that the purely inorganic halide perovskites are responsive to temperature, varying a lot in their crystal structures and hence optical properties [76, 77]. In 2018, Yang's group reported a novel smart solar window utilizing the caesium-based perovskite ($CsPbI_{3-x}Br_x$) thin film [78]. Figure 7.11d shows the thermochromic phase transition of $CsPbI_{3-x}Br_x$. Once reaching a critical transition temperature (as low as 105 °C), the structural rearrangement occurs in the $CsPbI_{3-x}Br_x$ crystal: from a colourless room temperature non-perovskite phase (low-T phase, 81.7% transparency) to an orange-red-coloured high-temperature perovskite phase (high-T phase, 35.4% transparency), as shown in Fig. 7.11e. The exposure to moisture can initiate the back-conversion of the high-T phase to low-T phase. Therefore, this perovskite-based smart solar

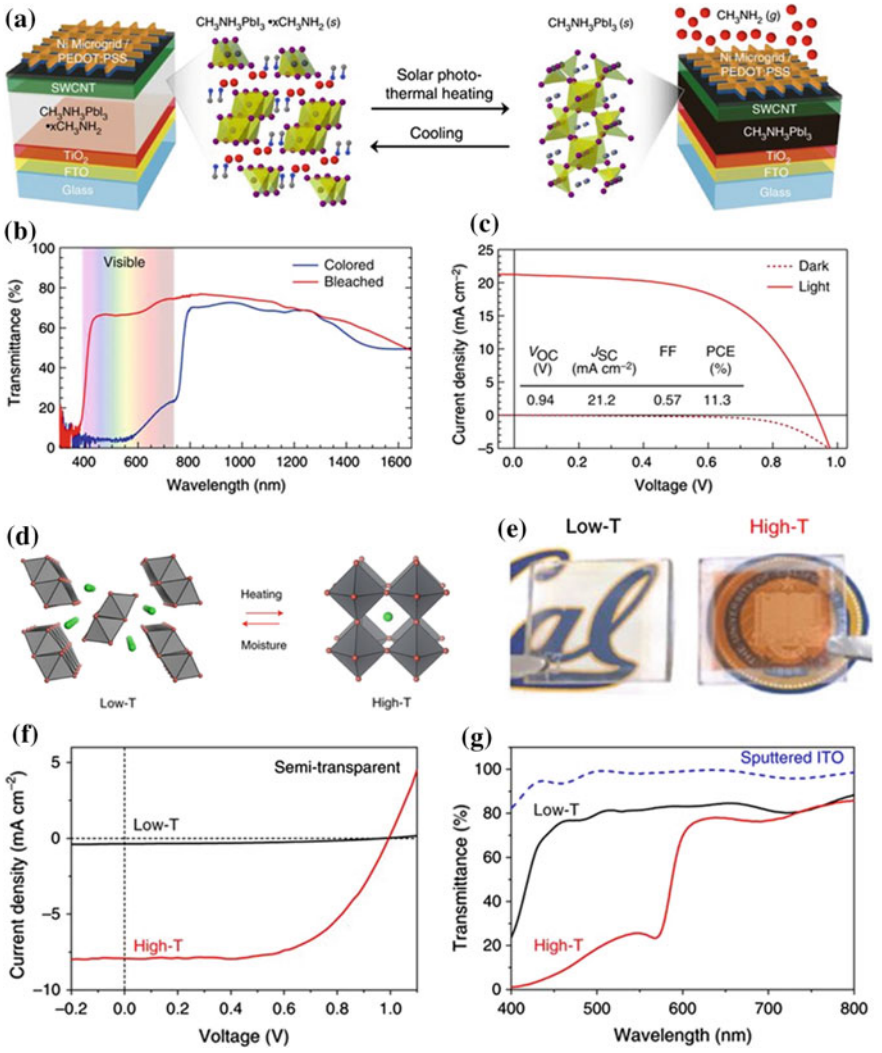

window can reversibly switch between a transparent low-temperature state with low-power output and a deeply coloured high-temperature state with high-energy output (conversion efficiency ≈ 7%) (Fig. 7.11f, g).

In spite of the fascinating features, the stability and efficiency of the perovskite-based smart solar windows are still far from satisfaction at the current stage. Wheeler's window, which is driven by chemical reaction, suffers from poor stability due to the loss of methylamine during the repetitive switching back and forth. Yang's structure transition-driven window, however, is limited by slow response (>10 h) and high transition temperature (>100 °C). In addition, both perovskite windows fail to

◀**Fig. 7.11** Halide perovskite smart solar windows based on the complexion–dissociation of methylamine (**a**–**c**) and the temperature-responsive structural change (**d**–**g**). **a** Schematic of the smart solar window architecture and the chemical reaction-induced thermochromism. In the architecture, TiO_2 is the electron transport layer, and fluorine-doped tin oxide (FTO) is the transparent conducting electrode. The single-walled carbon nanotube (SWCNT) is to provide hole extraction and improve lateral electrical transport. The topmost layer (microgrid/PEDOT:PSS) serves as an electric glue to package the whole device. **b** Transmittance spectra of the smart solar window in the transparent (red) and opaque (blue) states. It is obvious that the visible transmittance sharply drops after the dissociation of methylamine from the perovskite. **c** Current density versus voltage curve of the switchable smart solar window in the dark (dashed) and under illumination (solid). Reproduction from [75] with permission from Nature Publishing Group, Copyright 2017. **d** Schematic of the thermally driven, moisture-mediated reversible phase transition between the high-T and low-T phases. **e** The picture of the $CsPbIBr_2$ smart solar window in the colourless low-T state (left) and deeply coloured high-T state (right). The sputtered indium tin oxide (ITO) layer acts as the top transparent electrodes. **f** Current density versus voltage curve of the device. **g** The transmittance spectra of the smart solar windows at low-T (black) and high-T state (red). The spectrum for the sputtered ITO layer is as a reference. Reproduction from [78] with permission from Nature Publishing Group, Copyright 2018

regulate the light transmittance in the NIR range. Nevertheless, it is expected the smart solar windows will keep evolving with the persistent pursuit for new modified perovskites.

7.3 Responsive Nanomaterials for Electrochromic Smart Windows

Compared to the passive thermochromic windows with no energy input, electrochromic windows are powered by the electric supply, and they allow users to manage the light transmittance in a broad spectral range as needed by altering the applied voltage. Electrochromic materials are the core components in the whole device because they take control of the reversible redox switching between the bleached and coloured state as a response to electrical potential. To achieve the high optical performance of smart windows, electrochromic materials should provide high optical contrast, fast switching kinetics and high colouration efficiency [3]. Colouration efficiency is measured by the ratio of the optical absorbance change to the charge inserted into the electrochromic material per unit area [2]. In addition, the stability towards the long-term redox switching and sunlight exposure is of great importance. Various electrochromic materials, including transition metal oxides [79], conjugated polymers [80] and small organic and inorganic molecules [81, 82], have been employed in smart windows while they rarely reach a trade-off between optical performances, stability and production cost. These issues must be addressed, which is also the prerequisite for the commercialization of electrochromic smart windows. Numerous researches have proved that nanostructuring is an effective way to improve the conventional electrochromic materials [2, 3, 83]. Further,

the introduction of nanomaterials endows smart windows with new functionalities, which will greatly broaden their application in the energy saving and light managing. In section, we will focus on the well-studied nanostructured metal oxides and the emerging two-dimensional (2D) nanomaterials for electrochromic smart windows.

7.3.1 Metal Oxides-Based Electrochromic Nanomaterials

The use of transition metal oxides (TMOs), such as tungsten oxide (WO_3) [79], molybdenum oxide (MoO_3) [84] and titanium oxide (TiO_2) [85], in electrochromic devices dates back to 1960s when Deb first demonstrated the electrochromic phenomenon in WO_3 [86]. In the 1980s, the successful introduction of electrochromic WO_3 to the dynamic light modulating windows flourished the researches on the electrochromic smart windows [79, 87]. The electrochromic nature of TMOs originates from the reversible change in the oxidation state of transition metal ions with the insertion/extraction of electrons (e^-) and ions (M^+) upon voltage bias [88]. For example, the reversible electrochromism of WO_3 between the transparent and blue state is shown by the following Faradaic reaction [89]:

$$WO_3(\text{transparent}) + x\left(M^+ + e^-\right) \leftrightarrow M_x W^{VI}_{1-x} W^{V}_{x} O_3(\text{blue}) \tag{7.1}$$

In general, the colouration efficiency, optical contrast and response time are closely related to the amount of reduced/oxidized metal ions (colouration centres) and the kinetics of redox reaction. The electrochromic redox reactions of TMOs involve the charge transfer at the interface between electrolyte and TMOs and the ion diffusion controlled redox reaction within the lattice of TMOs. Typically, electrochromic thin films based on bulk TMOs fall short of colouration efficiency (in the range of tens cm^2/s) and response time (>60 s) due to impeded charge transfer and long ion diffusion distance [90]. Therefore, the facilitation and promotion of the two processes are key to improving the electrochromic performance. Herein, nanostructuring of TMOs, including nanoparticles [91–93], nanorods [94–96], nanosheets [97–99], nanowires [100, 101] and quantum dots [102, 103], has been proven as a potent route to expedite the processes and enhance the performance. Owing to the large specific surface area, nanostructured TMOs greatly facilitate the charge transfer on more metal ions. Further, the diffusion path for ions is considerably shortened, from micrometre to a few hundred or tens of nanometres, within the lattice of nanosized TMOs. The junction of these effects not only increases the total amount of colouration centres but also accelerates the overall kinetics of redox reactions, resulting in the deeper optical contrast, shorter switching time and higher colouration efficiency [90, 104]. It is also worth noting that nanostructured TMOs with higher colouration efficiency tend to have better durability because less charge is needed to produce a given span of optical modulation [2, 92]. In terms of economic benefit, solution-processable TMOs nanomaterials have advantages in improved manufacturability, inexpensive production and good compatibility with 3D printing techniques [6, 105–107].

Among all electrochromic TMOs, tungsten oxides have attracted the most extensive studies since Deb's pioneering work and, accordingly, much progress has been made in the nanostructured WO_3. In 2011, Zhang et al. developed a hexagonal WO_3 nanowire array film using a low-cost solvothermal method [108]. In the previous works, thermal evaporation and physical vapour deposition were the prevailing methods to synthesize WO_3 nanowires on the conducting substrates but these techniques are costly and energy-intensive [109, 110]. In Zhang's solvothermal method, the ordered WO_3 nanowires directly grew from WO_3 seeds on the transparent conductive FTO-coated glass by controlling the reaction conditions, such as pH and reactants. Compared with the WO_3 micro-brick film, improved electrochromic performance was observed in the resulting WO_3 nanowire array film, with high colouration efficiency of 102.8 cm^2/s and fast response time of 7.6 and 4.2 s for colouring and bleaching, respectively (Fig. 7.12a, b) [108]. Further enhancement in the electrochromic performance can be achieved by downsizing the nanocrystalline tungsten oxide to quantum dots (QDs) with an average size of 1.6 nm via a facile colloid process, as reported by Cong and his co-workers [103]. In addition to the efficient charge

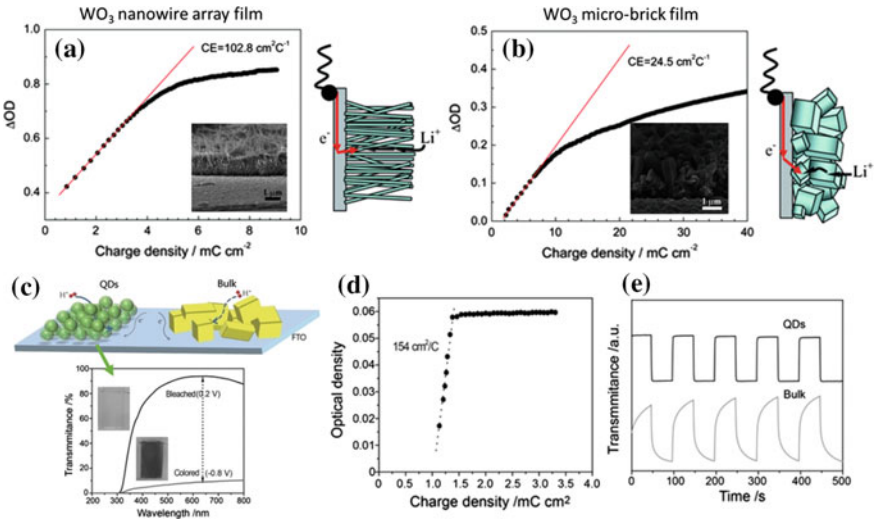

Fig. 7.12 Nanocrystalline WO_3 in the form of nanowires and quantum dots and the corresponding electrochromic performance. Colouration efficiency of WO_3 nanowire array film (**a**) and WO_3 micro-brick film (**b**). Reproduction from [108] with permission from Royal Society of Chemistry, Copyright 2011. **c** Tungsten oxide QDs provide more efficient ion diffusion and charge transfer than the bulk counterpart. Transmittance spectra for tungsten oxide QDs electrode deposited on FTO glass in the coloured (−0.8 V) and bleached (+0.2 V) states, respectively. The electrochromic window is highly transparent at bleached state (>90% of transmittance) and large modulation window (>80%). The insets are images of the electrode at bleached and coloured states, appearing almost transparent and dark blue colour, respectively. **d** The colouration efficiency of the QDs-based electrochromic window. **e** Alternate transmittance switching for bulk (green) and QDs (black) tungsten oxide showing significantly faster response for QDs. Reproduction from [103] with permission from Wiley-VCH, Copyright 2014

transfer and ion diffusion, tungsten oxide quantum dots are even more active in electrochromic reactions due to the ultrahigh proportion of surface atoms (Fig. 7.12c). Consequently, the QDs-based electrochromic window showed a remarkably high colouration efficiency (154 cm^2/s) and super-fast switching time (<1 s for both colouring and bleaching), as shown in Fig. 7.12d, e. The significant performance improvements can also be achieved in other TMOs at the nanoscale, such as TiO_2, [111] MoO_3 [84] and NiO [112].

In addition to the improved electrochromic performance, some nanostructured metal oxides with strong LSPR absorption can deliver a new functionality of selective NIR shielding to smart windows [113]. The LSPR effect can be flexibly tuned across a wide range of wavelengths by electrochemical charging or doping of plasmonic nanocrystals [2]. With the combination of intrinsic Faradaic reaction-based electrochromism and NIR-selective LSPR, the use of plasmonic nanocrystals allows the dynamic and independent control of NIR and visible light transmittance by varying the applied voltage, namely the dual-band electrochromism. In 2013, Milliron's group fabricated such a dual-band electrochromic window, for the first time, via incorporating the tin-doped indium oxide (ITO) nanocrystals into niobium oxide glass (NbO_x) [114]. Figure 7.13a illustrates the architecture and working principle of this smart window. The nanocrystal-in-glass composite electrode is coupled with a lithium counter electrode, both of which are immersed in the Li^+ electrolyte. Under the external bias, the amorphous NbO_x matrix modulates mostly the visible light while the ITO nanocrystals mainly block the NIR light through LSPR. As a whole, the nanocrystal-in-glass composite film progressively switches between three distinct operating modes: bright mode at the open-circuit voltage, cool mode at an intermediate voltage and dark mode at a low voltage (Fig. 7.13b). At bright mode, neither the insertion/extraction of Li^+ and electrons nor the LSPR happens, allowing the traverse of both visible and NIR light. At cool mode, the LSPR effect takes place in the charged ITO nanocrystals which have a sufficiently high concentration of free electrons, whereupon they only block most of NIR light while still welcome the visible light [115]. At dark mode, the electrochromic NbO_x comes into effect which results in the broadband blocking of NIR and visible light. Moreover, relative to the pure NbO_x film, the ITO-NbO_x composite is more durable and has better visible light modulation ability. This dual-band electrochromic smart window is more energy efficient than conventional smart windows owing to its controllable and selective regulation of solar heat exchange and interior lighting. Inspired by Milliron's work, the recent five years have witnessed the spring up of various metal oxide nanocomposite-based dual-band electrochromic smart windows [116–119]. Apart from the nanocomposite system, a single-component metal oxide nanocrystals with defects or dopants can also be utilized as an active material for this smart window [120–122]. For example, Lee's group reported a dual-band electrochromic smart window which exhibited bright mode at 1 V, cool mode at −2.8 V and dark mode at −4 V (as shown in Fig. 7.13c, d) [123]. Designed based on the monoclinic oxygen-deficient WO_3 (m-WO_{3-x}) nanowires, this smart window makes use of the LSPR property of m-WO_{3-x} nanowires and the phase transition (from dielectric and metallic) to modulate the NIR transmittance and the bandgap transitions (intraband

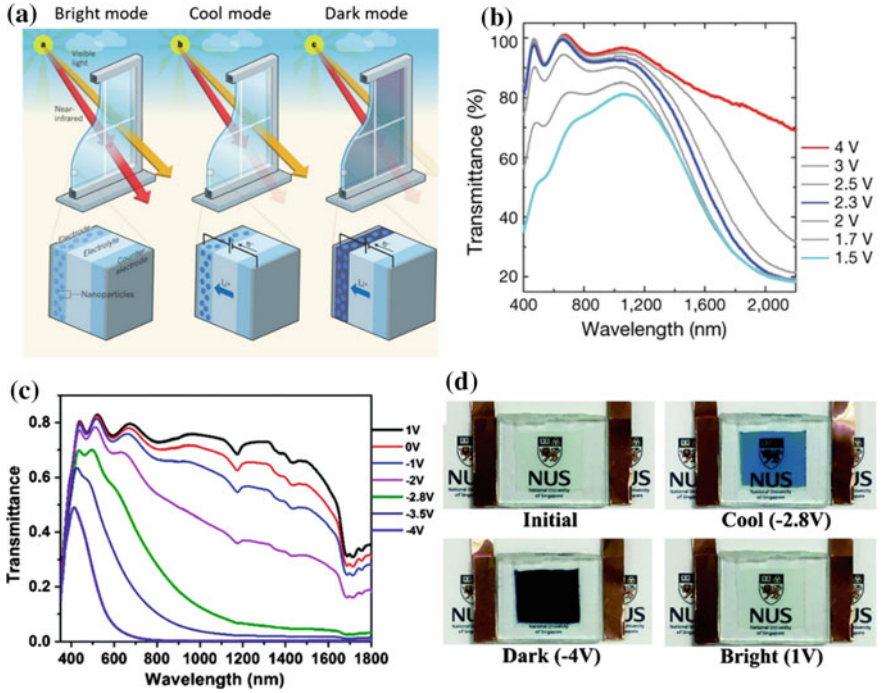

Fig. 7.13 Dual-band smart windows which can dynamically and independently manage the transmission of visible and NIR light. **a** The smart window based on plasmonic nanocrystal-in-glass exhibits three distinct modes. Reproduction from [125] with permission from Nature Publishing Group, Copyright 2013. **b** Changes in the transmittance spectra of the ITO-in-NbO_x film with the varying voltages versus Li/Li^+. The composite shows bright mode at 4 V, cool mode at 2.3 V and dark mode at 1.5 V. Reproduction from [114] with permission from Nature Publishing Group, Copyright 2013. **c** The transmittance spectra of the m-WO_{3-x} nanowires-based dual-band smart window under different external biases. **d** The three modes under different voltages. Reproduction from [123] with permission from Royal Society of Chemistry, Copyright 2018

and interband transition) to the visible transmittance. In addition, they replaced the commonly used monovalent Li^+ with the smaller multivalent Al^{3+} as the insertion ions and thus the smart window can deliver excellent solar light modulation ability, high colouration efficiencies (254 and 121 cm^2/C at NIR and visible region, respectively), fast response time (within 2 s for colouration/bleaching at NIR and visible region) and good stability and cyclability. The dual-band electrochromic smart windows are especially advantageous in the selective modulation of solar irradiation without sacrificing the visible transmittance for daylighting, helpful to reduce the energy consumption on HVAC and interior lighting [3, 124].

7.3.2 2D Electrochromic Nanomaterials

Since the first isolation of graphene in 2004 [126] atomically, thin 2D materials have been the spotlight of fundamental research and state-of-the-art technology due to their extraordinary electrical, mechanical, optical and chemical properties [127–131]. The uniqueness of 2D materials derives from the confinement of electrons and photons within their nanoscale thickness, which is much less than their lateral dimensions [132]. The recent in-depth research and exploration unearth the interesting optoelectronic properties of 2D materials, which can be made use of in the novel electrochromic applications.

As the best-known example of 2D materials, mono- or few-layered graphene is an ideal alternative to the traditional ITO transparent conductive electrode in the electrochromic windows due to its high mechanical strength, optical transparency and carrier mobility [133, 134]. The optical transparency tends to decrease with the number of graphene layers [135]. However, multilayered graphene will reveal a significant increase in optical transmittance and/or electrical conductivity towards the intercalation of foreign species, such as $FeCl_3$, Li^+ and Na^+, between the neighbouring layers (Fig. 7.14a) [136–139]. The principle behind this exceptional phenomenon is that intercalation heavily dopes graphene, which fills up the conduction band (higher electrical conductivity) and suppresses interband optical transitions by Pauli blocking (higher visible transmittance) [137]. The controllable and reversible intercalation of graphene can be achieved by electrochemical methods [132, 140]. For example, Bao et al. fabricated an encapsulated electrochemical cell in which the multilayered CVD graphene electrode received Li^+ from the Li counter electrode, and hence, Li^+ intercalation was enabled. As shown in Fig. 7.14b, c, the transparency of 40 and 80 nm thick graphene increases pronouncedly upon the external voltage is applied. Therefore, electrochemical intercalation of graphene potentially provides an emerging and promising strategy for making a simply structured electrochromic device with tunable transparency. In this device, graphene acts not only as a transparent conductive electrode but also as an active electrochromic contributor.

In 2015, Wan and his co-workers demonstrated such a reversible electrochromic device based on the electrochemical Na^+ intercalation of reduced graphene oxide (rGO) network (Fig. 7.14d, e) [139]. Its optical transmittance increases from 36 to 79% within 10 min when the Na^+ intercalation reaches its maximum (Fig. 7.14f). In comparison with Bao's work, they adopted the low-cost rGO as the dual-functional component instead of the costly CVD graphene. In addition, rGO has expanded interlayer spacing due to the presence of some oxygenated function groups which greatly facilitates the insertion of Na^+. Moreover, although both Na^+ and Li^+ are both highly reactive, this Na^+ intercalation electrochromic system is much more stable in air than Bao's Li^+ intercalation system. This is possibly related to the poorer diffusivity of Na^+ in the barrier layer at the edge of rGO sheets formed by the reaction between Na^+ and water/O_2/CO_2, thus well protecting the intercalated Na^+ inside the sheets. This electrochromic Na^+-intercalated rGO system provides a good example for the commercial intercalated graphene electrochromic windows in

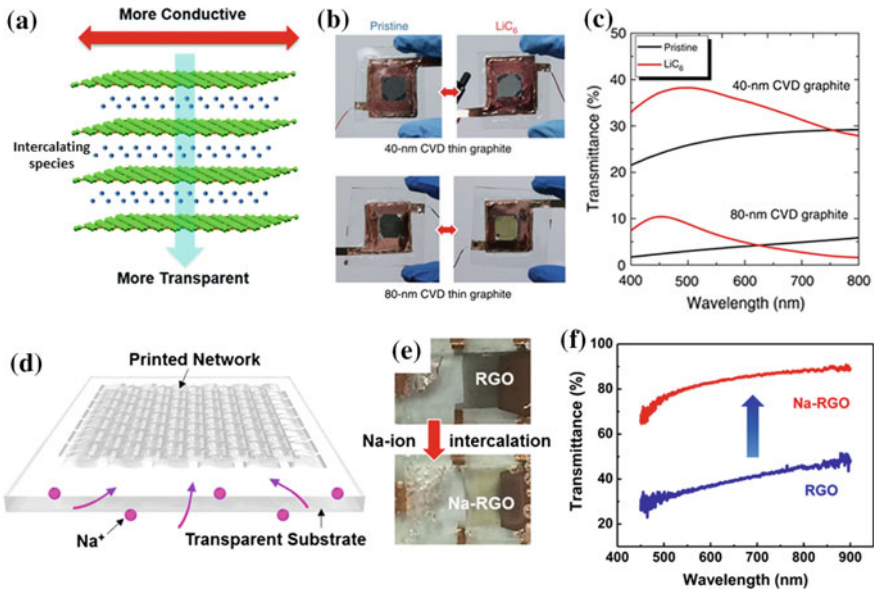

Fig. 7.14 Intercalated graphene-based electrochromic device. **a** Schematic of the multilayered graphene intercalated by metal ions. Reproduction from [132] with permission from Royal Society of Chemistry, Copyright 2016. **b** Images of the encapsulated CVD graphene electrochromic device with different thickness of graphene electrode. **c** The optical transmittance before and after the Li^+ intercalation. Both CVD graphene electrodes showed increased transparency after applying the external voltage to the devices. Reproduction from [137] with permission from Nature Publishing Group, Copyright 2014. **d** Schematic of Na^+ intercalation in the rGO film on the transparent substrate. **e** The images show the transparency increase in the Na^+-intercalated rGO electrochromic device. **f** The optical transmittance of rGO film before and after Na^+ intercalation. Reproduction from [139] with permission from American Chemical Society, Copyright 2015

the future. In addition to graphene, the intercalation-induced reversible change in the light transmittance also occurs in 2D molybdenum disulphide (MoS_2) and titanium carbide MXene flakes [141–143]. This type of 2D materials-based electrochromic devices is still at the very initial stage but holds great promise for low-cost and high-efficiency smart windows.

7.4 Conclusion and Outlook

Smart windows are appealing to green energy-saving buildings and smart home systems because of their dynamic management of light transmittance and solar heat exchange controlled by temperature (thermochromic) or users' preferences (electrochromic). After decades of development, thermochromic and electrochromic smart windows have obtained the preliminary success in commercialization, but their

high cost restricted their applications to high-end markets, e.g. the auto-dimming aeroplane windows. Thus, to promote the widespread adoption of smart windows, it is imperative to further lower the production cost, improve the performance and durability and enhance the energy-saving benefits. As discussed in this chapter, nanomaterials and nanotechnologies have considerable potential for enabling the broader commercialization of smart windows, ascribed to the numerous advantages offered by them. Firstly, the solution-processable nanomaterials are compatible with low cost and scalable wet chemical processes, including sol-gel, hydrothermal and electrochemical approaches. The feasible and flexible control of the composition, morphology and structure of nanomaterials in the wet chemical processes greatly facilitate the optimization of smart windows. The excellent solution processability also makes the as-prepared nanomaterials amendable to ink formulations for 3D printings and applications on various surfaces. Secondly, nanocrystallization and nanostructuring of responsive materials can contribute to the improved thermochromic and electrochromic properties, for example, greater ΔT_{solar} and T_{lum} in thermochromic windows and the deeper and faster switching in electrochromic windows, and the better stability and durability. In particular, nanomaterials with unique properties can even introduce new functionality to smart windows, such as the electrical power generation and the independent control of visible and NIR light. Lastly, nanomaterials-based smart windows are expected to be much more efficient in saving energy consumed for HVAC than the static glazed windows or conventional blinds, consequently compensating the relatively higher priced smart windows.

Despite the advantages of the utilization of nanomaterials, some fundamental issues must be addressed before further development and large-scale commercialization of smart windows can be realised. In terms of the wet chemical synthesis of nanomaterials, one of the major challenges is the level of defects which is more difficult to control than the more expensive chemical vapour deposition methods. The presence of unwanted defects might degrade the performance and durability of smart windows. In addition, it is still problematic to scale up the synthesis of nanocrystals because the increased thermal input in the industrial-level production will drastically influence the nanocrystal growth, different from the laboratory-scale synthesis, which is undesirable for smart windows [2]. Although multiple challenges are still awaiting solutions, the recent encouraging advances in the nanomaterials-powering smart windows point to a promising future in this field, which provides the possibility of achieving greater market penetration and commercial success in the near future.

References

1. Y. Gao, H. Luo, Z. Zhang, L. Kang, Z. Chen, J. Du, M. Kanehira, C. Cao, Nanoceramic VO_2 thermochromic smart glass: a review on progress in solution processing. Nano Energy **1**(2), 221–246 (2012)

2. E.L. Runnerstrom, A. Llordés, S.D. Lounis, D.J. Milliron, Nanostructured electrochromic smart windows: traditional materials and NIR-selective plasmonic nanocrystals. Chem. Commun. **50**(73), 10555–10572 (2014)
3. Y. Wang, E.L. Runnerstrom, D.J. Milliron, Switchable materials for smart windows. Annu. Rev. Chem. Biomol. Eng. **7**(1), 283–304 (2016)
4. M.E.A. Warwick, R. Binions, Advances in thermochromic vanadium dioxide films. J. Mater. Chem. A **2**(10), 3275–3292 (2014)
5. C. Costa, C. Pinheiro, I. Henriques, C.A.T. Laia, Inkjet printing of sol-gel synthesized hydrated tungsten oxide nanoparticles for flexible electrochromic devices. ACS Appl. Mater. Interfaces **4**(3), 1330–1340 (2012)
6. M. Layani, P. Darmawan, W.L. Foo, L. Liu, A. Kamyshny, D. Mandler, S. Magdassi, P.S. Lee, Nanostructured electrochromic films by inkjet printing on large area and flexible transparent silver electrodes. Nanoscale **6**(9), 4572–4576 (2014)
7. H. Ji, D. Liu, H. Cheng, C. Zhang, Inkjet printing of vanadium dioxide nanoparticles for smart windows. J. Mater. Chem. C **6**(10), 2424–2429 (2018)
8. Y. Cui, Y. Ke, C. Liu, Z. Chen, N. Wang, L. Zhang, Y. Zhou, S. Wang, Y. Gao, Y. Long, Thermochromic VO_2 for energy-efficient smart windows. Joule **2**(9), 1707–1746 (2018)
9. A. Seeboth, D. Lötzsch, R. Ruhmann, O. Muehling, Thermochromic polymers—function by design. Chem. Rev. **114**(5), 3037–3068 (2014)
10. J.H. Day, Thermochromism of inorganic compounds. Chem. Rev. **68**(6), 649–657 (1968)
11. Z. Lu, C. Li, Y. Yin, Synthesis and thermochromic properties of vanadium dioxide colloidal particles. J. Mater. Chem. **21**(38), 14776–14782 (2011)
12. S.M. Babulanam, T.S. Eriksson, G.A. Niklasson, C.G. Granqvist, Thermochromic VO_2 films for energy-efficient windows. Solar Energy Mater. **16**(5), 347–363 (1987)
13. P. Baum, D.-S. Yang, A.H. Zewail, 4D visualization of transitional structures in phase transformations by electron diffraction. Science **318**(5851), 788–792 (2007)
14. K.H. Warnick, B. Wang, S.T. Pantelides, Hydrogen dynamics and metallic phase stabilization in VO_2. Appl. Phys. Lett. **104**(10), 101913 (2014)
15. T.D. Manning, I.P. Parkin, M.E. Pemble, D. Sheel, D. Vernardou, Intelligent window coatings: atmospheric pressure chemical vapor deposition of tungsten-doped vanadium dioxide. Chem. Mater. **16**(4), 744–749 (2004)
16. L.Q. Mai, B. Hu, T. Hu, W. Chen, E.D. Gu, Electrical property of Mo-doped VO_2 nanowire array film by melting–quenching sol–gel method. J. Phys. Chem. B **110**(39), 19083–19086 (2006)
17. Y. Ke, C. Zhou, Y. Zhou, S. Wang, S.H. Chan, Y. Long, Emerging thermal-responsive materials and integrated techniques targeting the energy-efficient smart window application. Adv. Funct. Mater. **28**(22), 1800113 (2018)
18. G. Xu, P. Jin, M. Tazawa, K. Yoshimura, Tailoring of luminous transmittance upon switching for thermochromic VO_2 films by thickness control. Jpn. J. Appl. Phys. **43**(1), 186–187 (2004)
19. H.K. Raut, V.A. Ganesh, A.S. Nair, S. Ramakrishna, Anti-reflective coatings: a critical, in-depth review. Energy Environ. Sci. **4**(10), 3779–3804 (2011)
20. J. Zheng, S. Bao, P. Jin, TiO_2(R)/VO_2(M)/TiO_2(A) multilayer film as smart window: combination of energy-saving, antifogging and self-cleaning functions. Nano Energy **11**, 136–145 (2015)
21. G. Xu, P. Jin, M. Tazawa, K. Yoshimura, Optimization of antireflection coating for VO_2-based energy efficient window. Sol. Energy Mater. Sol. Cells **83**(1), 29–37 (2004)
22. H. Koo, D. Shin, S.-H. Bae, K.-E. Ko, S.-H. Chang, C. Park, The effect of CeO_2 antireflection layer on the optical properties of thermochromic VO_2 film for smart window system. J. Mater. Eng. Perform. **23**(2), 402–407 (2014)
23. Y. Gao, S. Wang, H. Luo, L. Dai, C. Cao, Y. Liu, Z. Chen, M. Kanehira, Enhanced chemical stability of VO_2 nanoparticles by the formation of SiO_2/VO_2 core/shell structures and the application to transparent and flexible VO_2-based composite foils with excellent thermochromic properties for solar heat control. Energy Environ. Sci. **5**(3), 6104–6110 (2012)

24. Z. Chen, C. Cao, S. Chen, H. Luo, Y. Gao, Crystallised mesoporous TiO_2(A)–VO_2(M/R) nanocomposite films with self-cleaning and excellent thermochromic properties. J. Mater. Chem. A **2**(30), 11874–11884 (2014)
25. L. Kang, Y. Gao, H. Luo, Z. Chen, J. Du, Z. Zhang, Nanoporous thermochromic VO_2 films with low optical constants, enhanced luminous transmittance and thermochromic properties. ACS Appl. Mater. Interfaces **3**(2), 135–138 (2011)
26. Y. Choi, D.M. Sim, Y.H. Hur, H.J. Han, Y.S. Jung, Synthesis of colloidal VO_2 nanoparticles for thermochromic applications. Sol. Energy Mater. Sol. Cells **176**, 266–272 (2018)
27. Z. Zhang, Y. Gao, Z. Chen, J. Du, C. Cao, L. Kang, H. Luo, Thermochromic VO_2 thin films: solution-based processing, improved optical properties, and lowered phase transformation temperature. Langmuir **26**(13), 10738–10744 (2010)
28. Y. Gao, C. Cao, L. Dai, H. Luo, M. Kanehira, Y. Ding, Z.L. Wang, Phase and shape controlled VO_2 nanostructures by antimony doping. Energy Environ. Sci. **5**(9), 8708–8715 (2012)
29. K. Laaksonen, S.Y. Li, S.R. Puisto, N.K.J. Rostedt, T. Ala-Nissila, C.G. Granqvist, R.M. Nieminen, G.A. Niklasson, Nanoparticles of TiO_2 and VO_2 in dielectric media: conditions for low optical scattering, and comparison between effective medium and four-flux theories. Sol. Energy Mater. Sol. Cells **130**, 132–137 (2014)
30. Z. Chen, Y. Gao, L. Kang, C. Cao, S. Chen, H. Luo, Fine crystalline VO_2 nanoparticles: synthesis, abnormal phase transition temperatures and excellent optical properties of a derived VO_2 nanocomposite foil. J. Mater. Chem. A **2**(8), 2718–2727 (2014)
31. T. Moot, C. Palin, S. Mitran, J.F. Cahoon, R. Lopez, Designing plasmon-enhanced thermochromic films using a vanadium dioxide nanoparticle elastomeric composite. Adv. Opt. Mater. **4**(4), 578–583 (2016)
32. Y. Naoi, J. Amano, Optimization of VO_2 nanowire polymer composite thermochromic films by optical simulation. J. Appl. Phys. **120**(23), 235301 (2016)
33. S.-Y. Li, G.A. Niklasson, C.G. Granqvist, Nanothermochromics: calculations for VO_2 nanoparticles in dielectric hosts show much improved luminous transmittance and solar energy transmittance modulation. J. Appl. Phys. **108**(6), 063525 (2010)
34. C.G. Granqvist, P.C. Lansåker, N.R. Mlyuka, G.A. Niklasson, E. Avendaño, Progress in chromogenics: new results for electrochromic and thermochromic materials and devices. Sol. Energy Mater. Sol. Cells **93**(12), 2032–2039 (2009)
35. Y. Chen, X. Zeng, J. Zhu, R. Li, H. Yao, X. Cao, S. Ji, P. Jin, High performance and enhanced durability of thermochromic films using VO_2@ZnO core-shell nanoparticles. ACS Appl. Mater. Interfaces **9**(33), 27784–27791 (2017)
36. S.-Y. Li, G.A. Niklasson, C.G. Granqvist, Nanothermochromics with VO_2-based core-shell structures: calculated luminous and solar optical properties. J. Appl. Phys. **109**(11), 113515 (2011)
37. Y. Ke, X. Wen, D. Zhao, R. Che, Q. Xiong, Y. Long, Controllable fabrication of two-dimensional patterned VO_2 nanoparticle, nanodome, and nanonet arrays with tunable temperature-dependent localized surface plasmon resonance. ACS Nano **11**(7), 7542–7551 (2017)
38. K. Manthiram, A.P. Alivisatos, Tunable localized surface plasmon resonances in tungsten oxide nanocrystals. J. Am. Chem. Soc. **134**(9), 3995–3998 (2012)
39. N. Wang, M. Duchamp, C. Xue, R.E. Dunin-Borkowski, G. Liu, Y. Long, Single-crystalline W-doped VO_2 nanobeams with highly reversible electrical and plasmonic responses near room temperature. Adv. Mater. Interfaces **3**(15), 1600164 (2016)
40. J. Zhu, Y. Zhou, B. Wang, J. Zheng, S. Ji, H. Yao, H. Luo, P. Jin, Vanadium dioxide nanoparticle-based thermochromic smart coating: high luminous transmittance, excellent solar regulation efficiency, and near room temperature phase transition. ACS Appl. Mater. Interfaces **7**(50), 27796–27803 (2015)
41. Y. Zhou, A. Huang, Y. Li, S. Ji, Y. Gao, P. Jin, Surface plasmon resonance induced excellent solar control for VO_2@SiO_2 nanorods-based thermochromic foils. Nanoscale **5**(19), 9208–9213 (2013)

42. Y. Ke, Y. Yin, Q. Zhang, Y. Tan, P. Hu, S. Wang, Y. Tang, Y. Zhou, X. Wen, S. Wu, T.J. White, J. Yin, J. Peng, Q. Xiong, D. Zhao, Y. Long, Adaptive thermochromic windows from active plasmonic elastomers. Joule **3**(3), 858–871 (2019)
43. J. Cao, E. Ertekin, V. Srinivasan, W. Fan, S. Huang, H. Zheng, J.W.L. Yim, D.R. Khanal, D.F. Ogletree, J.C. Grossman, J. Wu, Strain engineering and one-dimensional organization of metal–insulator domains in single-crystal vanadium dioxide beams. Nat. Nanotechnol. **4**, 732 (2009)
44. X. Cao, N. Wang, J.Y. Law, S.C.J. Loo, S. Magdassi, Y. Long, Nanoporous thermochromic VO_2 (M) thin films: controlled porosity, largely enhanced luminous transmittance and solar modulating ability. Langmuir **30**(6), 1710–1715 (2014)
45. M. Zhou, J. Bao, M. Tao, R. Zhu, Y. Lin, X. Zhang, Y. Xie, Periodic porous thermochromic VO_2(M) films with enhanced visible transmittance. Chem. Commun. **49**(54), 6021–6023 (2013)
46. M. Liu, B. Su, Y.V. Kaneti, Z. Chen, Y. Tang, Y. Yuan, Y. Gao, L. Jiang, X. Jiang, A. Yu, Dual-phase transformation: spontaneous self-template surface-patterning strategy for ultra-transparent VO_2 solar modulating coatings. ACS Nano **11**(1), 407–415 (2017)
47. C. Ba, S.T. Bah, M. D'Auteuil, P.V. Ashrit, R. Vallée, Fabrication of high-quality VO_2 thin films by ion-assisted dual ac magnetron sputtering. ACS Appl. Mater. Interfaces **5**(23), 12520–12525 (2013)
48. J.P. Fortier, B. Baloukas, O. Zabeida, J.E. Klemberg-Sapieha, L. Martinu, Thermochromic VO_2 thin films deposited by HiPIMS. Sol. Energy Mater. Sol. Cells **125**, 291–296 (2014)
49. J.-C. Orlianges, J. Leroy, A. Crunteanu, R. Mayet, P. Carles, C. Champeaux, Electrical and optical properties of vanadium dioxide containing gold nanoparticles deposited by pulsed laser deposition. Appl. Phys. Lett. **101**(13), 133102 (2012)
50. R. Binions, G. Hyett, C. Piccirillo, I.P. Parkin, Doped and un-doped vanadium dioxide thin films prepared by atmospheric pressure chemical vapour deposition from vanadyl acetylacetonate and tungsten hexachloride: the effects of thickness and crystallographic orientation on thermochromic properties. J. Mater. Chem. **17**(44), 4652–4660 (2007)
51. M.E.A. Warwick, C.W. Dunnill, J. Goodall, J.A. Darr, R. Binions, Hybrid chemical vapour and nanoceramic aerosol assisted deposition for multifunctional nanocomposite thin films. Thin Solid Films **519**(18), 5942–5948 (2011)
52. H. Yin, K. Yu, C. Song, Z. Wang, Z. Zhu, Low-temperature CVD synthesis of patterned core–shell VO_2@ZnO nanotetrapods and enhanced temperature-dependent field-emission properties. Nanoscale **6**(20), 11820–11827 (2014)
53. D. Li, W. Huang, L. Song, Q. Shi, Thermal stability of VO_2 thin films deposited by sol–gel method. J. Sol-Gel. Sci. Technol. **75**(1), 189–197 (2015)
54. J. Wu, W. Huang, Q. Shi, J. Cai, D. Zhao, Y. Zhang, J. Yan, Effect of annealing temperature on thermochromic properties of vanadium dioxide thin films deposited by organic sol–gel method. Appl. Surf. Sci. **268**, 556–560 (2013)
55. L. Kang, Y. Gao, H. Luo, A novel solution process for the synthesis of VO_2 thin films with excellent thermochromic properties. ACS Appl. Mater. Interfaces **1**(10), 2211–2218 (2009)
56. H. Watanabe, Intelligent window using a hydrogel layer for energy efficiency. Sol. Energy Mater. Sol. Cells **54**(1), 203–211 (1998)
57. H.G. Schild, D.A. Tirrell, Microcalorimetric detection of lower critical solution temperatures in aqueous polymer solutions. J. Phys. Chem. **94**(10), 4352–4356 (1990)
58. K. Jain, R. Vedarajan, M. Watanabe, M. Ishikiriyama, N. Matsumi, Tunable LCST behavior of poly(N-isopropylacrylamide/ionic liquid) copolymers. Polym. Chem. **6**(38), 6819–6825 (2015)
59. C. Wu, S. Zhou, Laser light scattering study of the phase transition of poly(N-isopropylacrylamide) in Water. 1. Single Chain. Macromolecules **28**(24), 8381–8387 (1995)
60. Y.-S. Yang, Y. Zhou, F.B.Y. Chiang, Y. Long, Tungsten doped VO_2/microgels hybrid thermochromic material and its smart window application. RSC Adv. **7**(13), 7758–7762 (2017)
61. T.-G. La, X. Li, A. Kumar, Y. Fu, S. Yang, H.-J. Chung, Highly flexible, multipixelated thermosensitive smart windows made of tough hydrogels. ACS Appl. Mater. Interfaces **9**(38), 33100–33106 (2017)

62. Y. Zhou, Y. Cai, X. Hu, Y. Long, Temperature-responsive hydrogel with ultra-large solar modulation and high luminous transmission for "smart window" applications. J. Mater. Chem. A **2**(33), 13550–13555 (2014)
63. H.Y. Lee, Y. Cai, S. Bi, Y.N. Liang, Y. Song, X.M. Hu, A dual-responsive nanocomposite toward climate-adaptable solar modulation for energy-saving smart windows. ACS Appl. Mater. Interfaces **9**(7), 6054–6063 (2017)
64. Y. Zhou, Y. Cai, X. Hu, Y. Long, VO_2/hydrogel hybrid nanothermochromic material with ultra-high solar modulation and luminous transmission. J. Mater. Chem. A **3**(3), 1121–1126 (2015)
65. V.R. de la Rosa, P. Woisel, R. Hoogenboom, Supramolecular control over thermoresponsive polymers. Mater. Today **19**(1), 44–55 (2016)
66. D. Kim, E. Lee, H.S. Lee, J. Yoon, Energy efficient glazing for adaptive solar control fabricated with photothermotropic hydrogels containing graphene oxide. Sci. Rep. **5**, 7646 (2015)
67. X. Li, D. Bi, C. Yi, J.-D. Décoppet, J. Luo, S.M. Zakeeruddin, A. Hagfeldt, M. Grätzel, A vacuum flash–assisted solution process for high-efficiency large-area perovskite solar cells. Science **353**(6294), 58–62 (2016)
68. M.M. Lee, J. Teuscher, T. Miyasaka, T.N. Murakami, H.J. Snaith, Efficient hybrid solar cells based on meso-superstructured organometal halide perovskites. Science **338**(6107), 643–647 (2012)
69. M. Liu, M.B. Johnston, H.J. Snaith, Efficient planar heterojunction perovskite solar cells by vapour deposition. Nature **501**, 395 (2013)
70. M. Grätzel, The light and shade of perovskite solar cells. Nat. Mater. **13**, 838 (2014)
71. M. De Bastiani, M.I. Saidaminov, I. Dursun, L. Sinatra, W. Peng, U. Buttner, O.F. Mohammed, O.M. Bakr, Thermochromic perovskite inks for reversible smart window applications. Chem. Mater. **29**(8), 3367–3370 (2017)
72. M.I. Saidaminov, A.L. Abdelhady, B. Murali, E. Alarousu, V.M. Burlakov, W. Peng, I. Dursun, L. Wang, Y. He, G. Maculan, A. Goriely, T. Wu, O.F. Mohammed, O.M. Bakr, High-quality bulk hybrid perovskite single crystals within minutes by inverse temperature crystallization. Nat. Commun. **6**, 7586 (2015)
73. G. Maculan, A.D. Sheikh, A.L. Abdelhady, M.I. Saidaminov, M.A. Haque, B. Murali, E. Alarousu, O.F. Mohammed, T. Wu, O.M. Bakr, $CH_3NH_3PbCl_3$ single crystals: inverse temperature crystallization and visible-blind UV-photodetector. J. Phys. Chem. Lett. **6**(19), 3781–3786 (2015)
74. C.C. Stoumpos, C.D. Malliakas, M.G. Kanatzidis, Semiconducting tin and lead iodide perovskites with organic cations: phase transitions, high mobilities, and near-infrared photoluminescent properties. Inorg. Chem. **52**(15), 9019–9038 (2013)
75. L.M. Wheeler, D.T. Moore, R. Ihly, N.J. Stanton, E.M. Miller, R.C. Tenent, J.L. Blackburn, N.R. Neale, Switchable photovoltaic windows enabled by reversible photothermal complex dissociation from methylammonium lead iodide. Nat. Commun. **8**(1), 1722 (2017)
76. C.K. MØller, Crystal structure and photoconductivity of cæsium plumbohalides. Nature **182**(4647), 1436 (1958)
77. S. Sharma, N. Weiden, A. Weiss, Phase diagrams of quasibinary systems of the type: ABX3—A′BX3; ABX3—AB′X3, and ABX3—ABX′3; X = Halogen. Z. Phys. Chem. (Muenchen, Ger.) **175**, 63 (1992)
78. J. Lin, M. Lai, L. Dou, C.S. Kley, H. Chen, F. Peng, J. Sun, D. Lu, S.A. Hawks, C. Xie, F. Cui, A.P. Alivisatos, D.T. Limmer, P. Yang, Thermochromic halide perovskite solar cells. Nat. Mater. **17**(3), 261–267 (2018)
79. G.A. Niklasson, C.G. Granqvist, Electrochromics for smart windows: thin films of tungsten oxide and nickel oxide, and devices based on these. J. Mater. Chem. **17**(2), 127–156 (2007)
80. C.M. Amb, A.L. Dyer, J.R. Reynolds, Navigating the color palette of solution-processable electrochromic polymers. Chem. Mater. **23**(3), 397–415 (2011)
81. H.C. Moon, T.P. Lodge, C.D. Frisbie, Solution processable, electrochromic ion gels for Sub-1 V, flexible displays on plastic. Chem. Mater. **27**(4), 1420–1425 (2015)

82. M. Stolar, J. Borau-Garcia, M. Toonen, T. Baumgartner, Synthesis and tunability of highly electron-accepting, N-benzylated "phosphaviologens". J. Am. Chem. Soc. **137**(9), 3366–3371 (2015)
83. Y. Li, H. Qu, Z. Tong, J. Zhao, Nanostructured electrochromic materials, in *Electrochromic Smart Materials: Fabrication and Applications* (The Royal Society of Chemistry, 2019), pp. 430–474
84. L. Zheng, Y. Xu, D. Jin, Y. Xie, Novel metastable hexagonal MoO_3 nanobelts: synthesis, photochromic, and electrochromic properties. Chem. Mater. **21**(23), 5681–5690 (2009)
85. R. Cinnsealach, G. Boschloo, S. Nagaraja Rao, D. Fitzmaurice, Coloured electrochromic windows based on nanostructured TiO_2 films modified by adsorbed redox chromophores. Sol. Energy Mater. Sol. Cells **57**(2), 107–125 (1999)
86. S.K. Deb, A novel electrophotographic system. Appl. Opt. **8**(S1), 192–195 (1969)
87. J.S.E.M. Svensson, C.G. Granqvist, Electrochromic coatings for "smart windows". Solar Energy Mater. **12**(6), 391–402 (1985)
88. W. Wu, M. Wang, J. Ma, Y. Cao, Y. Deng, Electrochromic metal oxides: recent progress and prospect. Adv. Electron. Mater. **4**(8), 1800185 (2018)
89. R.J. Mortimer, Electrochromic materials. Annu. Rev. Mater. Res. **41**(1), 241–268 (2011)
90. V.K. Thakur, G. Ding, J. Ma, P.S. Lee, X. Lu, Hybrid materials and polymer electrolytes for electrochromic device applications. Adv. Mater. **24**(30), 4071–4096 (2012)
91. Y.-Y. Song, Z.-D. Gao, J.-H. Wang, X.-H. Xia, R. Lynch, Multistage coloring electrochromic device based on TiO_2 nanotube arrays modified with WO_3 nanoparticles. Adv. Funct. Mater. **21**(10), 1941–1946 (2011)
92. S.-H. Lee, R. Deshpande, P.A. Parilla, K.M. Jones, B. To, A.H. Mahan, A.C. Dillon, Crystalline WO_3 nanoparticles for highly improved electrochromic applications. Adv. Mater. **18**(6), 763–766 (2006)
93. G. Cai, X. Wang, M. Cui, P. Darmawan, J. Wang, A.L.-S. Eh, P.S. Lee, Electrochromo-supercapacitor based on direct growth of NiO nanoparticles. Nano Energy **12**, 258–267 (2015)
94. R.S. Devan, S.-Y. Gao, W.-D. Ho, J.-H. Lin, Y.-R. Ma, P.S. Patil, Y. Liou, Electrochromic properties of large-area and high-density arrays of transparent one-dimensional β-Ta_2O_5 nanorods on indium-tin-oxide thin-films. Appl. Phys. Lett. **98**(13), 133117 (2011)
95. G. Yuan, C. Hua, S. Khan, S. Jiang, Z. Wu, Y. Liu, J. Wang, C. Song, G. Han, Improved electrochromic performance of WO_3 films with size controlled nanorods. Electrochim. Acta **260**, 274–280 (2018)
96. R.A. Patil, R.S. Devan, J.-H. Lin, Y.-R. Ma, P.S. Patil, Y. Liou, Efficient electrochromic properties of high-density and large-area arrays of one-dimensional NiO nanorods. Sol. Energy Mater. Sol. Cells **112**, 91–96 (2013)
97. A. Azam, J. Kim, J. Park, T.G. Novak, A.P. Tiwari, S.H. Song, B. Kim, S. Jeon, Two-dimensional WO_3 nanosheets chemically converted from layered WS_2 for high-performance electrochromic devices. Nano Lett. **18**(9), 5646–5651 (2018)
98. Z. Bi, X. Li, Y. Chen, X. He, X. Xu, X. Gao, Large-scale multifunctional electrochromic-energy storage device based on tungsten trioxide monohydrate nanosheets and prussian white. ACS Appl. Mater. Interfaces **9**(35), 29872–29880 (2017)
99. D. Ma, G. Shi, H. Wang, Q. Zhang, Y. Li, Hierarchical NiO microflake films with high coloration efficiency, cyclic stability and low power consumption for applications in a complementary electrochromic device. Nanoscale **5**(11), 4808–4815 (2013)
100. C. Xiong, A.E. Aliev, B. Gnade, K.J. Balkus, Fabrication of silver vanadium oxide and V_2O_5 nanowires for electrochromics. ACS Nano **2**(2), 293–301 (2008)
101. J.-L. Wang, Y.-R. Lu, H.-H. Li, J.-W. Liu, S.-H. Yu, Large area co-assembly of nanowires for flexible transparent smart windows. J. Chem. Soc. **139**(29), 9921–9926 (2017)
102. A. Hasani, Q.V. Le, M. Tekalgne, W. Guo, S.H. Hong, K.S. Choi, T.H. Lee, H.W. Jang, S.Y. Kim, Tungsten trioxide doped with CdSe quantum dots for smart windows. ACS Appl. Mater. Interfaces **10**(50), 43785–43791 (2018)
103. S. Cong, Y. Tian, Q. Li, Z. Zhao, F. Geng, Single-crystalline tungsten oxide quantum dots for fast pseudocapacitor and electrochromic applications. Adv. Mater. **26**(25), 4260–4267 (2014)

104. C.-P. Li, C.A. Wolden, A.C. Dillon, R.C. Tenent, Electrochromic films produced by ultrasonic spray deposition of tungsten oxide nanoparticles. Sol. Energy Mater. Sol. Cells **99**, 50–55 (2012)
105. G. Cai, P. Darmawan, X. Cheng, P.S. Lee, Inkjet printed large area multifunctional smart windows. Adv. Energy Mater. **7**(14), 1602598 (2017)
106. C.-W. Chang-Jian, E.-C. Cho, S.-C. Yen, B.-C. Ho, K.-C. Lee, J.-H. Huang, Y.-S. Hsiao, Facile preparation of WO_3/PEDOT:PSS composite for inkjet printed electrochromic window and its performance for heat shielding. Dyes Pigm. **148**, 465–473 (2018)
107. G. Cai, P. Darmawan, M. Cui, J. Chen, X. Wang, A.L.-S. Eh, S. Magdassi, P.S. Lee, Inkjet-printed all solid-state electrochromic devices based on NiO/WO_3 nanoparticle complementary electrodes. Nanoscale **8**(1), 348–357 (2016)
108. J. Zhang, J.-P. Tu, X.-H. Xia, X.-L. Wang, C.-D. Gu, Hydrothermally synthesized WO_3 nanowire arrays with highly improved electrochromic performance. J. Mater. Chem. **21**(14), 5492–5498 (2011)
109. J. Zhou, Y. Ding, S.Z. Deng, L. Gong, N.S. Xu, Z.L. Wang, Three-dimensional tungsten oxide nanowire networks. Adv. Mater. **17**(17), 2107–2110 (2005)
110. Y. Li, Y. Bando, D. Golberg, Quasi-aligned single-crystalline W18O49 nanotubes and nanowires. Adv. Mater. **15**(15), 1294–1296 (2003)
111. R.A. Patil, R.S. Devan, Y. Liou, Y.-R. Ma, Efficient electrochromic smart windows of one-dimensional pure brookite TiO_2 nanoneedles. Sol. Energy Mater. Sol. Cells **147**, 240–245 (2016)
112. S.-H. Lee, C.E. Tracy, Y. Yan, J.R. Pitts, S.K. Deb, Solid-State nanocomposite electrochromic pseudocapacitors. Electrochem. Solid-State Lett. **8**(4), A188–A190 (2005)
113. A. Agrawal, S.H. Cho, O. Zandi, S. Ghosh, R.W. Johns, D.J. Milliron, Localized surface plasmon resonance in semiconductor nanocrystals. Chem. Rev. **118**(6), 3121–3207 (2018)
114. A. Llordés, G. Garcia, J. Gazquez, D.J. Milliron, Tunable near-infrared and visible-light transmittance in nanocrystal-in-glass composites. Nature **500**, 323 (2013)
115. G. Garcia, R. Buonsanti, E.L. Runnerstrom, R.J. Mendelsberg, A. Llordes, A. Anders, T.J. Richardson, D.J. Milliron, Dynamically modulating the surface plasmon resonance of doped semiconductor nanocrystals. Nano Lett. **11**(10), 4415–4420 (2011)
116. A. Llordés, Y. Wang, A. Fernandez-Martinez, P. Xiao, T. Lee, A. Poulain, O. Zandi, C.A. Saez Cabezas, G. Henkelman, D.J. Milliron, Linear topology in amorphous metal oxide electrochromic networks obtained via low-temperature solution processing. Nat. Mater. **15**, 1267 (2016)
117. C.J. Barile, D.J. Slotcavage, M.D. McGehee, Polymer-nanoparticle electrochromic materials that selectively modulate visible and near-infrared light. Chem. Mater. **28**(5), 1439–1445 (2016)
118. J. Kim, G.K. Ong, Y. Wang, G. LeBlanc, T.E. Williams, T.M. Mattox, B.A. Helms, D.J. Milliron, Nanocomposite architecture for rapid, spectrally-selective electrochromic modulation of solar transmittance. Nano Lett. **15**(8), 5574–5579 (2015)
119. H. Gu, C. Guo, S. Zhang, L. Bi, T. Li, T. Sun, S. Liu, Highly efficient, near-infrared and visible light modulated electrochromic devices based on polyoxometalates and W18O49 nanowires. ACS Nano **12**(1), 559–567 (2018)
120. C.J. Dahlman, Y. Tan, M.A. Marcus, D.J. Milliron, Spectroelectrochemical signatures of capacitive charging and ion insertion in doped anatase titania nanocrystals. J. Am. Chem. Soc. **137**(28), 9160–9166 (2015)
121. S. Cao, S. Zhang, T. Zhang, Q. Yao, J.Y. Lee, A visible light-near-infrared dual-band smart window with internal energy storage. Joule **3**(4), 1152–1162 (2019)
122. S. Zhang, S. Cao, T. Zhang, Q. Yao, A. Fisher, J.Y. Lee, Monoclinic oxygen-deficient tungsten oxide nanowires for dynamic and independent control of near-infrared and visible light transmittance. Mater. Horiz. **5**(2), 291–297 (2018)
123. S. Zhang, S. Cao, T. Zhang, A. Fisher, J.Y. Lee, Al^{3+} intercalation/de-intercalation-enabled dual-band electrochromic smart windows with a high optical modulation, quick response and long cycle life. Energy Environ. Sci. **11**(10), 2884–2892 (2018)

124. N. DeForest, A. Shehabi, J. O'Donnell, G. Garcia, J. Greenblatt, E.S. Lee, S. Selkowitz, D.J. Milliron, United States energy and CO_2 savings potential from deployment of near-infrared electrochromic window glazings. Build. Environ. **89**, 107–117 (2015)
125. B.A. Korgel, Composite for smarter windows. Nature **500**, 278 (2013)
126. K.S. Novoselov, A.K. Geim, S.V. Morozov, D. Jiang, Y. Zhang, S.V. Dubonos, I.V. Grigorieva, A.A. Firsov, Electric field effect in atomically thin carbon films. Science **306**(5696), 666–669 (2004)
127. K. Novoselov, Mind the gap. Nat. Mater. **6**, 720 (2007)
128. M. Chhowalla, H.S. Shin, G. Eda, L.-J. Li, K.P. Loh, H. Zhang, The chemistry of two-dimensional layered transition metal dichalcogenide nanosheets. Nat. Chem. **5**, 263 (2013)
129. C. Lee, X. Wei, J.W. Kysar, J. Hone, Measurement of the elastic properties and intrinsic strength of monolayer graphene. Science **321**(5887), 385–388 (2008)
130. K.S. Kim, Y. Zhao, H. Jang, S.Y. Lee, J.M. Kim, K.S. Kim, J.-H. Ahn, P. Kim, J.-Y. Choi, B.H. Hong, Large-scale pattern growth of graphene films for stretchable transparent electrodes. Nature **457**, 706 (2009)
131. L. Gomez De Arco, Y. Zhang, C.W. Schlenker, K. Ryu, M.E. Thompson, C. Zhou, Continuous, highly flexible, and transparent graphene films by chemical vapor deposition for organic photovoltaics. ACS Nano **4**(5), 2865–2873 (2010)
132. J. Wan, S.D. Lacey, J. Dai, W. Bao, M.S. Fuhrer, L. Hu, Tuning two-dimensional nanomaterials by intercalation: materials, properties and applications. Chem. Soc. Rev. **45**(24), 6742–6765 (2016)
133. K. Mallikarjuna, H. Kim, Highly transparent conductive reduced graphene oxide/silver nanowires/silver grid electrodes for low-voltage electrochromic smart windows. ACS Appl. Mater. Interfaces **11**(2), 1969–1978 (2019)
134. J. Palenzuela, A. Viñuales, I. Odriozola, G. Cabañero, H.J. Grande, V. Ruiz, Flexible viologen electrochromic devices with low operational voltages using reduced graphene oxide electrodes. ACS Appl. Mater. Interfaces **6**(16), 14562–14567 (2014)
135. S. Bae, H. Kim, Y. Lee, X. Xu, J.-S. Park, Y. Zheng, J. Balakrishnan, T. Lei, H. Ri Kim, Y.I. Song, Y.-J. Kim, K.S. Kim, B. Özyilmaz, J.-H. Ahn, B.H. Hong, S. Iijima, Roll-to-roll production of 30-inch graphene films for transparent electrodes. Nat. Nanotechnol. **5**, 574 (2010)
136. I. Khrapach, F. Withers, T.H. Bointon, D.K. Polyushkin, W.L. Barnes, S. Russo, M.F. Craciun, Novel highly conductive and transparent graphene-based conductors. Adv. Mater. **24**(21), 2844–2849 (2012)
137. W. Bao, J. Wan, X. Han, X. Cai, H. Zhu, D. Kim, D. Ma, Y. Xu, J.N. Munday, H.D. Drew, M.S. Fuhrer, L. Hu, Approaching the limits of transparency and conductivity in graphitic materials through lithium intercalation. Nat. Commun. **5**, 4224 (2014)
138. K. Kanetani, K. Sugawara, T. Sato, R. Shimizu, K. Iwaya, T. Hitosugi, T. Takahashi, Ca intercalated bilayer graphene as a thinnest limit of superconducting C_6Ca. Proc. Natl. Acad. Sci. U. S. A. **109**(48), 19610–19613 (2012)
139. J. Wan, F. Gu, W. Bao, J. Dai, F. Shen, W. Luo, X. Han, D. Urban, L. Hu, Sodium-ion intercalated transparent conductors with printed reduced graphene oxide networks. Nano Lett. **15**(6), 3763–3769 (2015)
140. J. Wang, K.K. Manga, Q. Bao, K.P. Loh, High-yield synthesis of few-layer graphene flakes through electrochemical expansion of graphite in propylene carbonate electrolyte. J. Am. Chem. Soc. **133**(23), 8888–8891 (2011)
141. J. Wan, W. Bao, Y. Liu, J. Dai, F. Shen, L. Zhou, X. Cai, D. Urban, Y. Li, K. Jungjohann, M.S. Fuhrer, L. Hu, In situ investigations of Li-MoS_2 with planar batteries. Adv. Energy Mater. **5**(5), 1401742 (2015)
142. F. Xiong, H. Wang, X. Liu, J. Sun, M. Brongersma, E. Pop, Y. Cui, Li Intercalation in MoS_2: in situ observation of its dynamics and tuning optical and electrical properties. Nano Lett. **15**(10), 6777–6784 (2015)
143. K. Hantanasirisakul, M.-Q. Zhao, P. Urbankowski, J. Halim, B. Anasori, S. Kota, C.E. Ren, M.W. Barsoum, Y. Gogotsi, Fabrication of $Ti_3C_2T_x$ MXene transparent thin films with tunable optoelectronic properties. Adv. Electron. Mater. **2**(6), 1600050 (2016)